THE ASTROPHYSICAL JOURNAL, 539:L133–L136, 2000 August 20

LARGE-SCALE ^{13}CO $J = 5 \rightarrow 4$ AND [C I] MAPPING OF ORION A

R. PLUME,[1] F. BENSCH,[2] J. E. HOWE,[3] M. L. N. ASHBY,[1] E. A. BERGIN,[1] G. CHIN,[4] N. R. ERICKSON[3] P. F. GOLDSMITH,[5] M. HARWIT,[6] S. KLEINER,[1] D. G. KOCH,[7] D. A. NEUFELD,[8] B. M. PATTEN,[1] R. SCHIEDER,[2] R. L. SNELL,[3] J. R. STAUFFER,[1] V. TOLLS,[1] Z. WANG,[1] G. WINNEWISSER,[2] Y. F. ZHANG,[1] K. REYNOLDS,[9] R. JOYCE,[9] C. TAVOLETTI,[9] G. JACK,[9] C. J. RODKEY,[9] AND G. J. MELNICK[1]

Received 2000 February 2; accepted 2000 June 22; published 2000 August 16

ABSTRACT

We present maps of the ^{13}CO $J = 5 \rightarrow 4$ (551 GHz) and [C I] $^3P_1 \rightarrow {}^3P_0$ (492 GHz) emission in the Orion A molecular cloud, covering a $0\overset{\circ}{.}5 \times 2^\circ$ area. A large velocity gradient (LVG) analysis of ^{13}CO $J = 5 \rightarrow 4$ and $J = 1 \rightarrow 0$ suggests that the gas temperatures in the northern part of OMC-1 (north of $\Delta\delta = -20'$) are ~45 K and are, on average, at least 20 K higher than those to the south. The average ^{13}CO column density is $\log (N/\mathrm{cm}^{-2}) = 16.4 \pm 0.3$ and is fairly constant throughout the cloud, even in the low-temperature region south of BN/KL. LVG modeling of the [C I] emission shows a typical C^0 column density of 2×10^{17} cm^{-2}, which yields a C/CO abundance ratio in the cloud of ~0.1 (rising to levels in excess of 0.5 at the cloud edges). Comparison of the Δ-variance (which measures spatial structure in a manner similar to a power spectrum) of the *Submillimeter Wave Astronomy Satellite* [C I], Five College Radio Astronomy Observatory ^{13}CO $J = 1 \rightarrow 0$, and CS $J = 1 \rightarrow 0$ velocity-integrated maps suggests that the [C I] and ^{13}CO emission arise from the same gas. In contrast, the CS emission likely originates in gas that is considerably more clumpy.

Subject headings: ISM: abundances — ISM: clouds — ISM: individual (Orion) — ISM: molecules — stars: formation

1. INTRODUCTION

The large-scale structure of Orion A has been the subject of many surveys: low-energy rotational transitions of ^{12}CO and ^{13}CO (e.g., Heyer et al. 1992; Castets et al. 1990; Bally et al. 1987; Maddalena et al. 1986), CS $J = 1 \rightarrow 0$ and $J = 2 \rightarrow 1$ (Tatematsu et al. 1993, 1998; Lada, Bally, & Stark 1991), continuum emission (350 μm: Lis et al. 1998; 450 and 850 μm: Johnstone & Bally 1999), and neutral carbon ([C I]: Ikeda et al. 1999). The [C I], ^{12}CO, and ^{13}CO studies show the overall distribution and morphology of the bulk of the gas in Orion A. However, with only the low-energy transitions, one cannot easily or accurately determine the physical conditions in the gas (i.e., the density and temperature) since these transitions cannot discriminate between high or low temperature and density. Studies of higher rotational transitions help, but these studies have been limited to small spatial scales (Howe et al. 1993; Schultz, Krügel, & Beckman 1992; Graf et al. 1990; Schmid-Burgk et al. 1989; Harris et al. 1987).

Using the *Submillimeter Wave Astronomy Satellite* (*SWAS*) we have mapped [C I] $^3P_1 \rightarrow {}^3P_0$ and, for the first time, ^{13}CO $J = 5 \rightarrow 4$ over large scales ($\sim 0\overset{\circ}{.}5 \times 2^\circ$) in the Orion A molecular cloud. Combined with observations of ^{13}CO $J = 1 \rightarrow 0$ and CS $J = 1 \rightarrow 0$, we are able to study the physical conditions of the gas over scales much larger than have been previously possible.

2. OBSERVATIONS

The *SWAS* observations presented in this Letter were taken between 1999 January and April. The observations within approximately $\pm 10'$ of the BN/KL object were made in a nodding mode (Melnick et al. 2000b). These observations contain ~40 minutes of on-source integration time per point and are described in Melnick et al. (2000a). The remainder of the observations were obtained in a mapping mode and contain ~2 minutes of on-source integration time per point. The beam spacing of the *SWAS* observations is $1'.6$ (half-beam spacing). For more information on the *SWAS* instrument, beam sizes, and data acquisition and reduction, see Melnick et al. (2000b).

The ^{13}CO $J = 1 \rightarrow 0$ observations were taken from 1999 February to May using the Five College Radio Astronomy Observatory (FCRAO) 14 m telescope. We used the 16-element SEQUOIA array receiver coupled with a digital autocorrelator back end. The bandwidth of the autocorrelator is 40 MHz, with a channel spacing of 78 kHz and a channel resolution of 94 kHz. The beam width is $47''$ (FWHM), and the map spacing is $44''$. All data are presented in units of T_A^*; however, to calculate densities and column densities the data are converted to main-beam temperatures (T_{mb}) using efficiencies of $\eta_{\mathrm{mb}} = 0.90$ for *SWAS* (Melnick et al. 2000b) and $\eta_{\mathrm{mb}} = 0.48$ for the FCRAO data. Unlike ground-based telescopes operating at submillimeter frequencies, the absence of an atmosphere and the great instrumental stability of *SWAS* ensure constant calibration for all the *SWAS* data.

3. RESULTS

Figures 1*a*–1*c* present our observations in the form of integrated intensity maps. The data comprising the maps in Figure 1 are presented at the intrinsic resolution of the telescopes (i.e., they are unsmoothed). They have, however, had linear

[1] Harvard-Smithsonian Center for Astrophysics, 60 Garden Street, Cambridge, MA 02138.
[2] I. Physikalisches Institut, Universität zu Köln, Zülpicher Strasse 77, D-50937 Köln, Germany.
[3] Department of Astronomy, University of Massachusetts, Amherst, MA 01003.
[4] NASA Goddard Space Flight Center, Greenbelt, MD 20771.
[5] National Astronomy and Ionosphere Center, Department of Astronomy, Cornell University, Ithaca, NY 14853-6801.
[6] 511 H Street SW, Washington, DC 20024-2725; also Cornell University.
[7] NASA Ames Research Center, Moffett Field, CA 94035.
[8] Department of Physics and Astronomy, Johns Hopkins University, 3400 North Charles Street, Baltimore, MD 21218.
[9] Keystone Oaks Planetarium, 1000 Kelton Avenue, Pittsburgh, PA 15216.

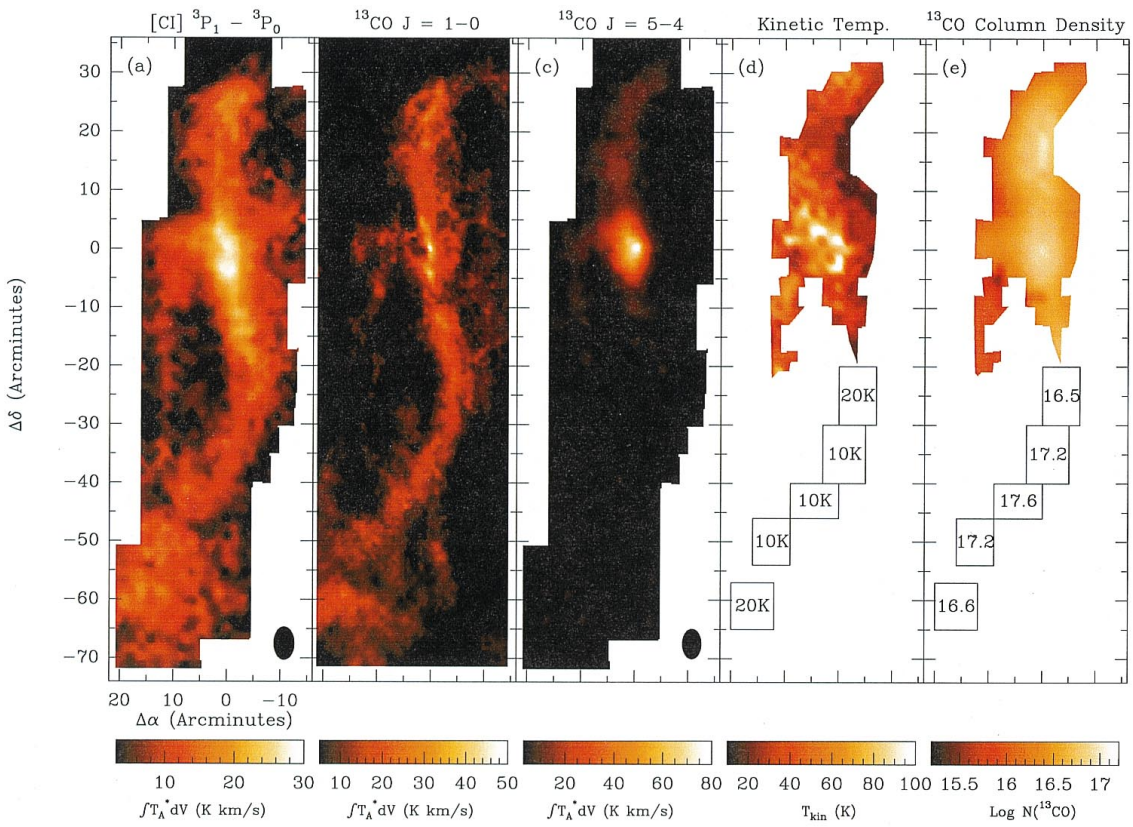

FIG. 1.—Observations and modeling results of the Orion A molecular cloud. Offsets are given with respect to the central position defined as $\alpha = 5^h35^m14^s.5$, $\delta = -5°22'37''$ (J2000). Ovals in the bottom right-hand corner of each panel indicate the beam size. A detailed description of each panel is as follows. (*a*) The integrated intensity ($\int T_A^* dV$) of the [C I] $^3P_1 \rightarrow {}^3P_0$ emission as observed by *SWAS*. (*b*) The ^{13}CO $J = 1 \rightarrow 0$ emission as observed by FCRAO. (*c*) The ^{13}CO $J = 5 \rightarrow 4$ emission as observed by *SWAS*. (*d*) Map of the gas kinetic temperature as determined by fitting the ^{13}CO $J = 1 \rightarrow 0$ and $J = 5 \rightarrow 4$ observations to LVG models (see § 4.1). The five boxes indicate the regions where spectra were co-added in order to produce higher signal-to-noise ratio ^{13}CO $J = 5 \rightarrow 4$ spectra. (*e*) Map of the ^{13}CO column density as determined from the LVG model fits.

order baselines subtracted. It is immediately apparent that, over large scales, the [C I] emission is extended and morphologically similar to the low-J ^{13}CO emission, a phenomenon that has been noted in other giant molecular clouds with nearby UV sources (Plume et al. 1999; Plume, Jaffe, & Keene 1994; Ikeda et al. 1999). The [C I] and ^{13}CO $J = 1 \rightarrow 0$ maps show the familiar integral-shaped filament (Bally et al. 1987), while the ^{13}CO $J = 5 \rightarrow 4$ emission is considerably less extended than the [C I] and the ^{13}CO $J = 1 \rightarrow 0$ emission. North of $\Delta\delta = -10'$, the ^{13}CO $J = 5 \rightarrow 4$ emission morphology is similar to that of the other two tracers. To the south, however, the ^{13}CO $J = 5 \rightarrow 4$ emission falls below detectable values. This suggests that the excitation conditions are considerably different in the southern part of the Orion A cloud (see § 4.1).

[C I] emission in the Orion A cloud has recently been mapped by the Mount Fuji telescope (Ikeda et al. 1999) with similar resolution. Comparing our [C I] and ^{13}CO $J = 1 \rightarrow 0$ integrated intensities, we find a correlation that is almost identical to that reported by Ikeda et al. (1999) and that is similar to those reported between [C I] and ^{13}CO $J = 2 \rightarrow 1$ (Tauber et al. 1995; Plume et al. 1999). In contrast, there is only a very weak correlation between the [C I] and ^{13}CO $J = 5 \rightarrow 4$ integrated intensities.

In the region south of $\Delta\delta = -20'$ we selected five separate regions (the five boxes in Figs. 1*d* and 1*e*) that follow the ^{13}CO $J = 1 \rightarrow 0$ emission. To improve the signal-to-noise ratio we then averaged all ^{13}CO $J = 5 \rightarrow 4$ spectra falling within each of these regions. Although no individual spectrum in these regions shows detectable ^{13}CO $J = 5 \rightarrow 4$ emission, the co-added spectra clearly show emission at this frequency. Figure 2 shows [C I], ^{13}CO $J = 1 \rightarrow 0$, and $J = 5 \rightarrow 4$ spectra from three representative positions in the Orion A cloud. The peak [C I] and ^{13}CO $J = 5 \rightarrow 4$ antenna temperatures (T_A^*) are 6.5 and 15.4 K, respectively. The average line widths (FWHM) are 2.4 and 2.7 km s^{-1} for [C I] and ^{13}CO $J = 5 \rightarrow 4$, respectively. Channel maps of the [C I] line clearly show that there is a large-scale velocity gradient in the cloud with LSR velocites ranging from ~7 km s^{-1} in the south to ~12 km s^{-1} in the north. The gradient in the [C I] line is similar to that noted from low-J ^{12}CO and ^{13}CO maps of the region (Heyer et al. 1992; Bally et al. 1987; Kutner et al. 1977).

4. DISCUSSION

4.1. *Large-scale Physical Conditions*

To determine the physical conditions in the Orion A molecular cloud we used a large velocity gradient (LVG) code to solve the coupled equations of radiative transfer and statistical equilibrium. We created a grid of LVG models with 20 column densities per unit velocity interval ($N/\Delta V = 5 \times 10^{14}$–$5 \times 10^{17}$ cm^{-2} (km s^{-1})$^{-1}$ and 10 values of the kinetic temperature (T_{kin} = 10–100 K). We selected a constant density of $n = 10^4$ cm^{-3} based on the large-scale observations of CS $J = 1 \rightarrow 0$ (Tatematsu et al. 1993) and $J = 2 \rightarrow 1$ (Tatematsu et al. 1998). Then, for each position in Orion A for which we have

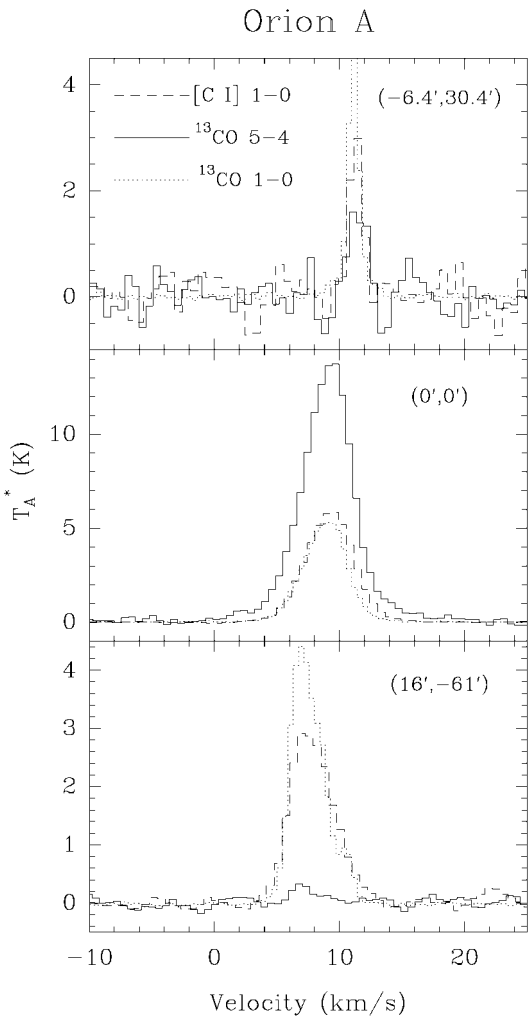

FIG. 2.—Plot showing spectra for the *SWAS* [C I] $J = 1 \rightarrow 0$ (*dashed line*) and ^{13}CO $J = 5 \rightarrow 4$ (*solid line*) transitions, and the FCRAO ^{13}CO $J = 1 \rightarrow 0$ (*dotted line*) transition at three representative positions within the Orion A cloud. The positions are (*from top to bottom*): the northernmost region mapped ($\Delta\alpha$, $\Delta\delta = -6\farcm4, +30\farcm4$), the BN/KL region ($\Delta\alpha, \Delta\delta = 0', 0'$), and the southernmost region mapped (a co-add of all spectra within $\pm 4'$ of $\Delta\alpha$, $\Delta\delta = +16'$, $-61'$). All spectra have been smoothed to the spatial and velocity resolution of the *SWAS* [C I] observations.

detectable ^{13}CO $J = 5 \rightarrow 4$ emission, we used a χ^2 minimization technique to find the LVG model that best reproduced our ^{13}CO $J = 1 \rightarrow 0$ and $J = 5 \rightarrow 4$ observations.

Figure 1*d* shows a map of the gas kinetic temperature as determined from LVG fits to the two ^{13}CO lines. The average gas temperature in this region is 43 ± 17 K. South of $\Delta\delta = -20'$, where there is no detectable ^{13}CO $J = 5 \rightarrow 4$ emission, we used the co-added spectra in the five boxes (Fig. 1*d*) to perform the LVG fitting. The gas temperatures derived using $n = 10^4$ cm^{-3} are displayed inside each of the boxes in Figure 1*d*, clearly demonstrating that the gas in the southern part of Orion A is, on average, 20 K colder than that in the northern part of the cloud. These gas kinetic temperatures are in general agreement with previous ^{12}CO observations, which show that the ^{12}CO $J = 1 \rightarrow 0$ peak temperatures south of BN/KL (~15 K) are colder than those to the north (>30 K; e.g., Heyer et al. 1992).

Figure 1*e* presents maps of the total ^{13}CO column density in the region as determined from our LVG analysis. The ^{13}CO column density is fairly constant throughout the region at $\log (N/\text{cm}^{-2}) = 16.4 \pm 0.3$ and remains at this level even in the southern part of the cloud, where the temperatures are considerably lower.

To estimate the sensitivity of the results on our assumption of a constant density throughout the cloud, we reran the LVG code for two additional cases: (1) a constant density of $\log (n/\text{cm}^{-3}) = 3.5$ and kinetic temperatures from 20 to 130 K and (2) a constant density of $\log (n/\text{cm}^{-3}) = 4.5$ and kinetic temperatures from 5 to 95 K. For $\log (n/\text{cm}^{-3}) = 3.5$ we find that the derived kinetic temperatures are significantly elevated (by 90%), whereas the column density decreases by 12%. For $\log (n/\text{cm}^{-3}) = 4.5$ we find $\Delta T_{\text{kin}} = -40\%$ and $\Delta N = +30\%$. Given the similarities between the peak ^{12}CO antenna temperatures and the kinetic temperatures derived here (for a constant density of 10^4 cm^{-3}), we feel this choice of density is appropriate.

To determine the neutral carbon (C^0) column density for each position, we assume a constant density of 10^4 cm^{-3} and use the kinetic temperature derived from the ^{13}CO LVG analysis. We then used our LVG code to find the C^0 column density that produced the best match to the observed [C I] line strength. In the region for which we were able to determine kinetic temperatures (Fig. 1*d*), the average C^0 column density ranges from $\sim 3 \times 10^{16}$ cm^{-2} to $\sim 5 \times 10^{17}$ cm^{-2} with an average of 2×10^{17} cm^{-2}. Single-sided, plane-parallel photodissociation region (PDR) models, which predict [C I] column densities of $\sim 2 \times 10^{17}$ cm^{-2} (Hollenbach, Takahashi, & Tielens 1991), are in good agreement with these results (assuming the [C I] emission arises from both the front and back sides of the cloud). Throughout the bulk of the cloud, the C^0/CO column density ratio is ~0.10 [assuming $N(\text{CO})/N(^{13}\text{CO}) = 55$]. However, as the ^{13}CO column density decreases, $N(C^0)/N(\text{CO})$ increases asymptotically to values that exceed 0.5. This asymptotic behavior (see Plume et al. 1999 for details) can also be reproduced by plane-parallel PDR models. Therefore, over large scales in Orion, there is no apparent need to invoke chemical bistability models (Le Bourlot, Pineau des Forêts, & Roueff 1993) to explain the observed C^0 column density and $N(C^0)/N(\text{CO})$ ratios, as has been suggested by Ikeda et al. (1999).

4.2. *Large-Scale Spatial and Velocity Structure*

We employed a Δ-variance analysis for a quantitative comparison of the structure visible in the line-integrated maps (Fig. 1). Introduced by Stutzki et al. (1998), the Δ-variance allows one to study the drift behavior of scalar functions, such as the spatial intensity variations in molecular cloud images. In particular, it provides information on the power spectrum of the image: for images with a power spectrum following a power law proportional to $k^{-\beta}$ [where $k = (k_x^2 + k_y^2)^{1/2}$ is the spatial frequency] and completely random phases of the Fourier amplitudes, the Δ-variance is a power law of the form $L^{\beta-2}$. Therefore, the Δ-variance is a function of the linear spatial scale L. An image with $\beta = 0$ represents pure white noise, i.e., the structure is dominated by spatially uncorrelated variations at the smallest scales. As β increases, the spatial intensity distribution becomes smoother; $\beta = 2$ represents a case where variations on all linear scales contribute equally to the observed intensity variations (here the area enclosed by the isointensity contours scales linearly with the perimeter of the contour). For images with $\beta \geq 4$, the spatial structure is dominated by large-scale variations of size close to the linear extent of the image. Previous studies of molecular cloud images using Δ-variance

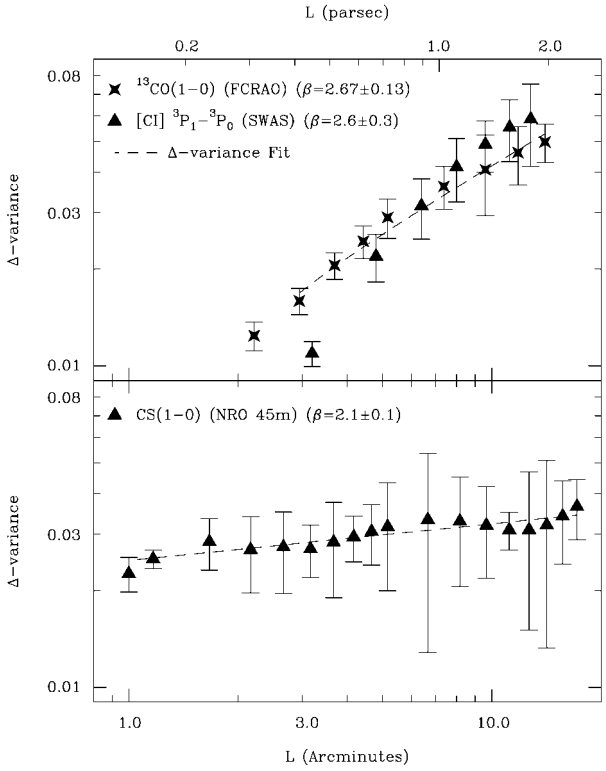

FIG. 3.—Δ-variance of the velocity-integrated spectral line maps observed in the [C I] and ^{13}CO $J = 1 \rightarrow 0$ transition (*top*) and the CS $J = 1 \rightarrow 0$ transition (*bottom*). A power law is fitted to the Δ-variance of each map, modified at the smaller angular scales to account for the noise in the maps and the finite angular resolution of the telescope. For the ^{13}CO $J = 1 \rightarrow 0$ map, the (noise and beam smearing) corrected Δ-variance is shown by the dashed line. For the linear scale given in the top panel of the figure we assume a distance to Orion A of 480 pc.

techniques typically give β between 2.5 and 3.5 (Stutzki et al. 1998; F. Bensch, J. Stutzki, & V. Ossenkopf 2000, in preparation). Contrary to the power spectrum, the Δ-variance can be determined purely in the spatial domain. Therefore, it is less vulnerable to edge effects than the Fourier transform (i.e., the power spectrum) of the image (F. Bensch et al. 2000, in preparation). In addition, a more accurate correction for the contribution of the white noise and the influence of the telescope beam is possible in a Δ-variance analysis.

The Δ-variance for the velocity-integrated *SWAS* [C I] and FCRAO ^{13}CO $J = 1 \rightarrow 0$ map is shown in the top panel of Figure 3. For angular scales $\gtrsim 5'$, the two curves follow each other closely (within the error bars). The deviation seen in the [C I] data toward smaller size scales is due to the larger beam of the *SWAS* telescope; the finite resolution of the telescope beam smooths the intensity variations at angular scales close to the beam FWHM and thus results in a smaller Δ-variance. A fit to the Δ-variance of the observed maps was done assuming a power law, modified at small angular scales because of the influence of noise and a Gaussian telescope beam (see F. Bensch et al. 2000, in preparation for details and the error treatment). Within the estimated accuracy, the power spectral indices β of the [C I] map ($\beta = 2.6 \pm 0.3$) and the ^{13}CO $J = 1 \rightarrow 0$ map ($\beta = 2.67 \pm 0.13$) are the same. In addition, these values are consistent with the spectral indices typically found for other large-scale molecular cloud images with a linear resolution larger than ~0.5 pc ($2.5 \leq \beta \leq 2.8$: F. Bensch et al. 2000, in preparation). In contrast, the Δ-variance for the CS $J = 1 \rightarrow 0$ map is significantly flatter (Fig. 3, *bottom*). A fit to the data gives a power spectral index of $\beta = 2.1 \pm 0.1$.

Our Δ-variance analysis suggests that the [C I] and ^{13}CO $J = 1 \rightarrow 0$ emitting material are closely linked, both dynamically and spatially. This is supported by an analysis of the structure seen in the individual channel maps of both data cubes, which will be presented in more detail in a forthcoming paper. The flatter Δ-variance (and thus flatter power spectrum) of the CS $J = 1 \rightarrow 0$ map indicates that the intensity distribution of the high-density tracer is much more inhomogeneous and disconnected. Compared to the ^{13}CO $J = 1 \rightarrow 0$ and [C I] maps, the flatter Δ-variance of the CS map at large scales indicates that the large-scale ordering in coherent structures is less pronounced for the CS-emitting gas. It indicates that the denser material traced by the CS line emission does not correlate well with the column density (as traced by the ^{13}CO $J = 1 \rightarrow 0$ emission). This suggests that the formation of each small, dense region traced by the CS emission is relatively independent and not coherent on larger linear scales ($\gtrsim 1$ pc).

We would like to thank Ken Tatematsu for the use of his CS data and the anonymous referee for his insightful comments. This work was supported by NASA grant NAS5-30702 (to *SWAS*) and NSF grant AST 97-25951 to the Five College Radio Astronomy Observatory. R. Schieder, G. Winnewisser, and F. Bensch would like to acknowledge the generous support provided by the DLR through grants 50 0090 090 and 50 0099 011.

REFERENCES

Bally, J., Langer, W. D., Stark, A. A., & Wilson, R. W. 1987, ApJ, 312, L45
Castets, A., Duvert, G., Dutrey, A., Bally, J., Langer, W. D., & Wilson, R. W. 1990, A&A, 234, 469
Graf, U. U., Genzel, R., Harris, A. I., Russell, A. P. G., & Stutzki, J. 1990, ApJ, 358, L49
Harris, A. I., Stutzki, J., Genzel, R., Lugten, J. B., Stacey, G. J., & Jaffe, D. T. 1987, ApJ, 322, L49
Heyer, M. H., Morgan, J., Schloerb, F. P., Snell, R. L., & Goldsmith, P. F. 1992, ApJ, 395, L99
Hollenbach, D. J., Takahashi, T., & Tielens, A. G. G. M. 1991, ApJ, 377, 192
Howe, J. E., Jaffe, D. T., Grossman, E. N., Wall, W. F., Mangum, J. G., & Stacey, G. J. 1993, ApJ, 410, 179
Ikeda, M., et al. 1999, ApJ, 527, L59
Johnstone, D., & Bally, J. 1999, ApJ, 510, L49
Kutner, M. L., Tucker, K. D., Chin, G., & Thaddeus, P. 1977, ApJ, 215, 521
Lada, E. A., Bally, J., & Stark, A. A. 1991, ApJ, 368, 432
Le Bourlot, J., Pineau des Forêts, G., & Roueff, E. 1993, ApJ, 416, L87
Lis, D. C., Serabyn, E., Keene, J., Dowell, C. D., Benford, D. J., Phillips, T. G., Hunter, T. R., & Wang, N. 1998, ApJ, 509, 299
Maddalena, R. J., Morris, M., Moscowitz, J., & Thaddeus, P. 1986, ApJ, 303, 375
Melnick, G., et al. 2000a, ApJ, 539, L87
———. 2000b, ApJ, 539, L77
Plume, R., Jaffe, D. T., & Keene, J. 1994, ApJ, 425, L49
Plume, R., Jaffe, D. T., Tatematsu, K., Evans, N. J., II, & Keene, J. 1999, ApJ, 512, 768
Schmid-Burgk, J., et al. 1989, A&A, 215, 150
Schultz, A., Krügel, E., & Beckmann, U. 1992, A&A, 264, 629
Stutzki, J., Bensch, F., Heithausen, A., Ossenkopf, V., & Zielinsky, M. 1998, A&A, 336, 697
Tatematsu, K., Umemoto, T., Heyer, M. H., Hirano, N., Kameya, O., & Jaffe, D. T. 1998, ApJS, 118, 517
Tatematsu, K., et al. 1993, ApJ, 404, 643
Tauber, J. A., Lis, D. C., Keene, J., Schilke, P., & Büttgenbach, T. H. 1995, A&A, 297, 567